2017

# Magnetically Ordered Transition-Metal-Intercalated $WSe_2$

Pankaj Kumar
*Boise State University*

Ralph Skomski
*University of Nebraska-Lincoln*, rskomski2@unl.edu

Raghani Pushpa
*Boise State University*

ACS OMEGA

Article

Cite This: ACS Omega 2017, 2, 7985-7990

http://pubs.acs.org/journal/acsodf

# Magnetically Ordered Transition-Metal-Intercalated $WSe_2$

Pankaj Kumar,*[,†] Ralph Skomski,[‡] and Raghani Pushpa[†]

[†]Department of Physics, Boise State University, 1910 University Dr., Boise, Idaho 83725, United States

[‡]Department of Physics and Astronomy and NCMN, University of Nebraska, Lincoln, Nebraska 68588, United States

**ABSTRACT:** Introducing magnetic behavior in nonmagnetic transition metal dichalcogenides is essential to broaden their applications in spintronic and nanomagnetic devices. In this article, we investigate the electronic and magnetic properties of transition-metal-intercalated tungsten diselenide ($WSe_2$) using density functional theory. We find that intercalation compounds with composition of $T_{1/4}WSe_2$ (T is an iron-series transition-metal atom) exhibit substantial magnetic moments and pronounced ferromagnetic order for late transition metals. The densities of states of the T atoms and the magnetic moments on the W sites indicate that the moments of the intercalated atoms become more localized with increasing atomic number. A large perpendicular magnetocrystalline anisotropy of about 9 meV per supercell has been found for $Fe_{1/4}WSe_2$. Furthermore, using mean field theory, we estimated high Curie temperatures of 660, 475, and 379 K for Cr, Mn, and Fe, respectively. The predicted magnetic properties suggest that $WSe_2$ may have applications in spin electronics and nanomagnetic devices.

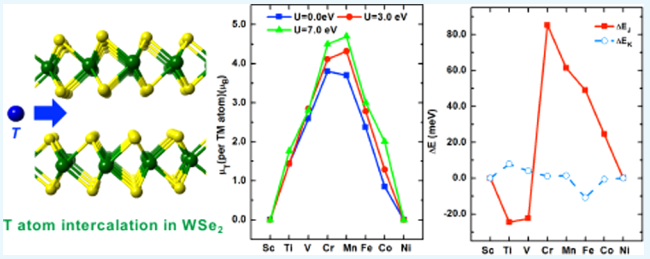


## 1. INTRODUCTION

Transition metal dichalcogenides (TMDs) have attracted much attention due to their intriguing physical and chemical properties, which stimulate intense research from both fundamental and technological viewpoints. The technological aspect includes applications in various fields, such as electronics, catalysis, photonics, and energy storage.[1−5] TMDs are quasi two-dimensional (2D) structures formed by stacking of $MX_2$ trilayers (M = transition metal, X = S, Se, Te) that are coupled by van der Waals (vdW) forces. However, the nonmagnetic nature of most TMDs prevents their applications in spin-electronic devices. Various approaches have been developed to induce and manipulate the magnetism in these materials, such as through point defects,[6,7] doping,[7−10] ion intercalation,[11−13] and strain.[14−17] Among these approaches, intercalation of foreign magnetic atoms is of significant interest as the atoms can be stored in the space between the TMD layers. The systems synthesized this way provide a unique opportunity to tuning their magnetic properties depending upon the nature and concentration of the intercalates.

Various spin structures are encountered in these magnetic intercalation compounds. For example, $M_{1/3}NbS_2$ is antiferromagnetic (AFM) with intercalated Fe, Co, and Ni atoms,[18] whereas $M_{1/3}TaS_2$ is ferromagnetic (FM) with a small Curie temperature.[19] Spintronic applications normally require large easy-axis magnetocrystalline anisotropy ($K_1 > 0$). Very recently, Ko et al.[13] observed a large unquenched orbital moment of 1 $\mu_B$ for Fe intercalates and a huge magnetocrystalline anisotropy of 15 meV per supercell in $Fe_{1/4}TaS_2$. Later, giant magnetoresistance and coercivity were observed in this system.[20,21] Mn-intercalated $TaS_2$ has also been found to be magnetic but with easy-plane anisotropy ($K_1 < 0$).[22]

The high anisotropy of $Fe_{1/4}TaS_2$ is a spin−orbit coupling (SOC) effect linked to the unquenched orbital moment.[13] In second-order perturbation theory, the anisotropy is proportional to $\xi\Delta\mu_L$, where $\xi$ is the spin−orbit coupling constant and $\Delta\mu_L$ is the change in orbital moment during spin rotation.[23,24] The SOC is particularly large in heavy elements, about 300 meV in the middle of the Pt (5d) series. The question therefore arises whether similar effects are caused by intercalated iron-series (3d) transition-metal atoms in other TMDs containing heavy elements. Among other TMDs, $WSe_2$ is another potential candidate, which exhibits pronounced spin−orbit effects in the absence of intercalated atoms.[25,26] Intercalation of alkaline and transition-metal atoms in $WSe_2$ has been investigated in the context of structural, electrical, optical, and photovoltaic applications.[27−31] However, magnetic properties of $WSe_2$ intercalated with 3d transition-metal elements are still under investigation and vital for future spintronic devices.

In this article, we investigate the magnetism of $WSe_2$ intercalated with transition-metal atoms. A comprehensive density-functional analysis of energetics and electronic and magnetic properties of series $T_{1/4}WSe_2$ has been performed, where T is the iron-series (3d) transition metal ranging from Sc to Ni. Depending on the intercalated transition-metal atom, the interaction between neighboring T atoms is ferromagnetic (FM) or antiferromagnetic (AFM). In particular, we find AFM order in $WSe_2$ for Ti and V intercalate atoms. For Cr, Mn, Fe, and Co, we find FM order and a large magnetic anisotropy for Mn and Fe intercalation.

**Received:** August 10, 2017
**Accepted:** November 3, 2017
**Published:** November 15, 2017




DOI: 10.1021/acsomega.7b01164
ACS Omega 2017, 2, 7985−7990

## 2. RESULTS AND DISCUSSION

As shown in Figure 1, the stoichiometry of the (1/4)T atom per $WSe_2$ formula unit can be realized using a 2 × 2 × 1

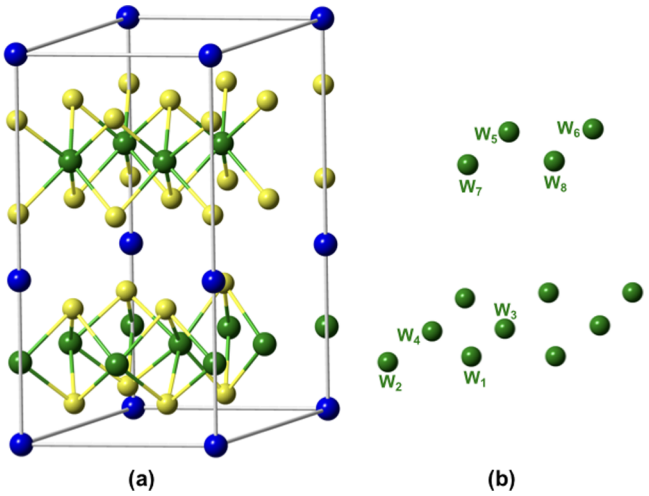


**Figure 1.** Structure of 3d-metal-intercalated $WSe_2$: (a) supercell of $[T_{1/4}WSe_2]_8$ and (b) indexed W layers in the supercell. The blue, green, and yellow spheres represent T (Sc to Ni), W, and Se atoms, respectively.

supercell, and the intercalated atoms are accommodated in the van der Waals gaps of the two layers of $WSe_2$. As a result of intercalation, the intermolecular forces between the neighboring TMD layers are expected to change from vdW to ionic, metallic, or covalent with the intercalate atom mediating the interaction.[32,33] Therefore, the results for transition-metal-intercalated $WSe_2$ are calculated without dispersion correction. There are more than one possibilities of realizing the $T_{1/4}WSe_2$ chemical composition in the supercell, and we chose the one having the lowest energy. Figure 1 shows the corresponding arrangement of the atoms in the $[T_{1/4}WSe_2]_8$ supercell. Each supercell contains eight formula units and therefore two T atoms.

Table 1 shows the optimized lattice parameters for $[WSe_2]_8$ intercalated with 3d transition-metal atoms. From the table, we

**Table 1. Optimized Lattice Constants $a = b$, Average Charge Transfer from T Atoms, Nearest T−T Distances, and Intercalation Energy per T Atom Intercalated in $T_{1/4}WSe_2$**

| T | $a$ (Å) | $c$ (Å) | charge transfer ($e$) | T−T distance (Å) | insertion energy (eV) |
|---|---|---|---|---|---|
| Sc | 6.733 | 14.316 | 1.569 | 6.805 | −4.15 |
| Ti | 6.739 | 14.242 | 1.238 | 6.433 | −3.65 |
| V | 6.705 | 14.401 | 0.942 | 6.115 | −3.10 |
| Cr | 6.697 | 14.618 | 0.830 | 6.242 | −1.94 |
| Mn | 6.712 | 14.185 | 0.780 | 5.965 | −1.72 |
| Fe | 6.680 | 13.953 | 0.676 | 5.869 | −2.61 |
| Co | 6.696 | 13.535 | 0.352 | 5.613 | −3.42 |
| Ni | 6.693 | 13.567 | 0.328 | 5.597 | −3.77 |

see that the intercalation increases the lattice constant, $c$, by up to 12%, whereas the effect on $a$ is insignificant (a maximum change of 2.5%). The lattice expansion in the $c$-direction reflects an increase in the W−Se bond length, which is a consequence of the large size of the intercalated atoms and of the charge transfer to the W and Se atoms. In more detail, $WSe_2$ layers interact via van der Waals forces, but this interaction changes to metallic upon intercalation. Furthermore, the intercalate atoms move toward neighboring W atoms. As a result, one layer of $WSe_2$ induces more polarization than that from the other. The corresponding in-plane atomic displacement is 3−5% for W ($W_1$ and $W_4$) atoms near the intercalate atoms, whereas this displacement is less than 2.5% for other atoms. Table 1 shows the corresponding charge transfers from the T intercalates to neighboring W and Se atoms. Furthermore, the charge transfer calculated using Bader charge analysis[34] shows that the guest atoms act as mediators for the interaction between the negatively charged $WSe_2$ layers.

To verify the feasibility of intercalation in $WSe_2$, we calculated the energy for inserting transition-metal atoms into $WSe_2$ using the following equation

$$E_{\text{insertion}} = 8E(T_{1/4}WSe_2) - 8E(WSe_2) - 2E(T) \quad (1)$$

where the energies refer to one supercell, that is, to two T atoms, and last term $E(T)$ corresponds to the total energy of an isolated T atom, which is computed by placing a T atom in a large supercell. The computed intercalation energies are tabulated in Table 1. From the table, we can infer that intercalation in $WSe_2$ is energetically favorable. This means that the T atoms remain captured between the dichalcogenide layers, rather than diffusing between the layers and recombining to yield precipitates of elemental metals.[5] In other words, intercalated compounds are more robust than atoms or molecules adsorbed on surfaces because of the thick and chemically inert TMD sheets surrounding the intercalate atoms.

Figure 2a,b shows the total spin magnetic moment ($\mu_{\text{tot}}$) and the spin moment per intercalated atom ($\mu_T$) of ferromagnetic

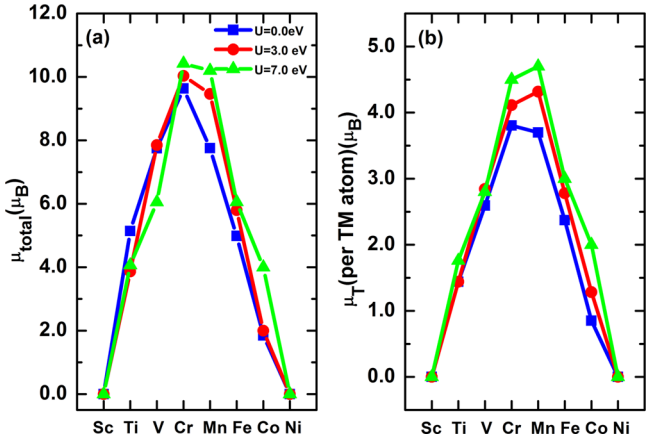


**Figure 2.** Spin magnetic moments as a function of transition-metal atom T in $[T_{1/4}WSe_2]_8$: (a) moment per unit cell and (b) moment on each T atom. The calculations have all been done for $U$ = 0.0, 3.0, and 7.0 eV, without spin−orbit interaction and with ferromagnetic T−T exchange.

$T_{1/4}WSe_2$, respectively, as a function of atomic number with and without including Hubbard terms $U$ = 3 and 7 eV and $J$ = 1 eV. The exact value of $U$ is unknown but probably close to 3 eV, and the blue and green lines in Figure 2 indicate that $U$ has a rather small effect on the magnetic moment. The total spin moments per supercell shown in Figure 2a slightly differ from twice of the transition-metal moment shown in Figure 2b. These differences arise due to the hybridization of iron-series 3d and W 5d moments, which partially spin-polarizes the



DOI: 10.1021/acsomega.7b01164
ACS Omega 2017, 2, 7985−7990

neighboring W atoms. In the case of Ti, V, and Cr guest atoms, the total spin moment is larger than $2\mu_T$, which indicates parallel spin alignment between neighboring transition-metal and W atoms, whereas for intercalated Mn, Fe, and Co atoms, the total moment is reduced due to antiparallel spin alignment with neighboring W atoms.

To gain quantum-mechanical insight into the nature of magnetism in intercalated $WSe_2$ systems, we plot the densities of states (DOSs) of intercalates, as shown in Figure 3. The Se

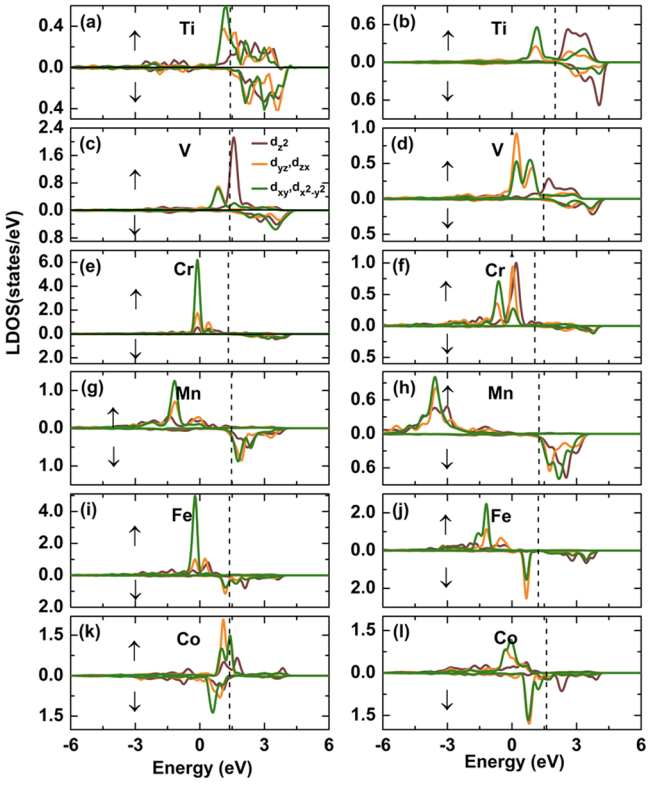


**Figure 3.** (a–l) Orbital-projected ferromagnetic partial density of states (DOS) of 3d metal atoms in $[T_{1/4}WSe_2]_8$ at $U$ = 0 eV (left panel) and $U$ = 3 eV (right panel). The Fermi levels are shown by vertical dashed lines.

atoms surrounding the T atom form a nearly distorted octahedron, due to which the 3d orbitals of T atoms split up into three levels, namely, (i) $d_z^2$, (ii) $d_{xy}$, $d_{x^2-y^2}$, and (iii) $d_{xz}$, $d_{yz}$, which are broadened by interatomic hopping. The d bands of intercalated atoms shown in Figure 3 lie in the band gap of the host material. The DOSs for Sc and Ni have not been shown here because Sc and Ni do not induce any magnetism. In case of Ti and V intercalates, the bands are delocalized and hybridized with neighboring W and Se atoms, resulting in a small ferromagnetic polarization in W, as shown in Figure 3a–d. The bands of Cr, on the other hand, are localized, as shown in Figure 3e. From Figure 3e, we find that the majority states of Cr are mostly filled, whereas minority states are empty. This produces a high magnetic moment in the Cr atoms. Note that the majority states of Ti, V, and Cr lie within the band gap of $WSe_2$, which produces a magnetic behavior in $Ti_{1/4}WSe_2$ and $V_{1/4}WSe_2$.

Figure 3g,i shows that the majority states of Mn and Fe are mostly filled, whereas the minority states are partially empty, which leads to large magnetic moments in $Mn_{1/4}WSe_2$. In case of Mn intercalation, the three sets of states $d_z^2$, ($d_{x^2-y^2}/d_{xy}$), and ($d_{yz}/d_{zx}$) are empty, as shown in Figure 3g, whereas for the Fe intercalate, as shown in Figure 3i, the $d_{x^2-y^2}/d_{xy}$ and $d_{yz}/d_{zx}$ levels are partially occupied.

Inclusion of Hubbard interaction parameter $U$ for this case pushes the states away from the Fermi level, as shown in Figure 3h,j, which increases the magnetic moment of Mn and Fe intercalates. For Co intercalation, the majority and minority states are mostly occupied, partially empty majority $d_z^2$ states, which yields a small magnetic moment in the Co intercalate. The inclusion of $U$ somewhat increases the number of unoccupied minority states. Note that $U$ is not exactly known for the present intercalates, and its accurate calculation goes beyond the scope of this article. The inclusion of $U$ has some effect on the magnetic moment but leaves the overall picture unchanged.

Table 2 lists the spin moments on the tungsten atoms. This relatively small moment, induced through interatomic hybrid-

**Table 2. Induced Spin Magnetic Moments ($\mu_B$) in Neighboring W Atoms in Ferromagnetic $[T_{1/4}WSe_2]_8$ without Hubbard-$U$**

| | Ti | V | Cr | Mn | Fe | Co |
|---|---|---|---|---|---|---|
| $W_1$ | 0.13 | 0.14 | 0.08 | 0.04 | 0.02 | 0.01 |
| $W_2$ | 0.04 | 0.21 | 0.03 | −0.13 | −0.1 | −0.13 |
| $W_3$ | 0.13 | 0.15 | 0.07 | 0.01 | 0.0 | 0.01 |
| $W_4$ | 0.16 | 0.16 | 0.06 | −0.02 | −0.01 | 0.03 |
| $W_5$ | 0.08 | 0.15 | 0.13 | −0.06 | −0.02 | −0.01 |
| $W_6$ | 0.03 | −0.03 | −0.01 | 0.02 | 0.01 | 0.01 |
| $W_7$ | 0.12 | 0.17 | 0.13 | −0.06 | −0.02 | −0.01 |
| $W_8$ | 0.00 | 0.17 | 0.12 | −0.06 | −0.01 | −0.01 |

ization by the iron-series atoms, is most pronounced for Ti and V but virtually negligible for Mn and Fe. This finding indicates that the magnetism of $Ti_{1/4}WSe_2$ and $V_{1/4}WSe_2$ is largely itinerant, the magnetic moment being delocalized all over the unit cell. By comparison, the moments of $Mn_{1/4}WSe_2$, $Fe_{1/4}WSe_2$, and $Fe_{1/4}WSe_2$ are more localized on the Mn and Fe sites, which limits the degree of 3d–5d hybridization and the corresponding induced W moment. The same conclusion can be drawn from the densities of states of Figure 3. As the atomic number of the T atoms increases, the 3d band narrows because the effective nuclear charge acting on the T atoms becomes larger toward the end of the iron series. This leads to a reduced interatomic hybridization, to narrower bands, and to reduced W moments.

To study the magnetic order in $T_{1/4}WSe_2$, we compared the total energies of antiferromagnetic (AFM) and ferromagnetic (FM) spin configurations. The AFM configuration is obtained by flipping one of the T spins in the supercell, similar to previous approximate calculations of exchange constants.[35,36] The AFM configuration chosen in this article is therefore the one in which neighboring T layers along the $z$-direction are aligned antiparallel and corresponds to minimum energy among different AFM configurations. Figure 4 shows the energy difference ($\Delta E_J = E^{AFM} - E^{FM}$) between the FM and AFM states across the iron series without SOC (red curve), whereas $\Delta E_K$ is the corresponding SOC correction (dashed blue). The Sc and Ni intercalates are nonmagnetic, which implies that there is no magnetic order. For Ti and V intercalates, we predict AFM order, whereas for Cr, Mn, Fe, and Co, we find FM order. The respective T moments in the AFM configurations, namely, 1.46, 2.70, 3.82, 3.74, 2.44, and



DOI: 10.1021/acsomega.7b01164
ACS Omega 2017, 2, 7985–7990

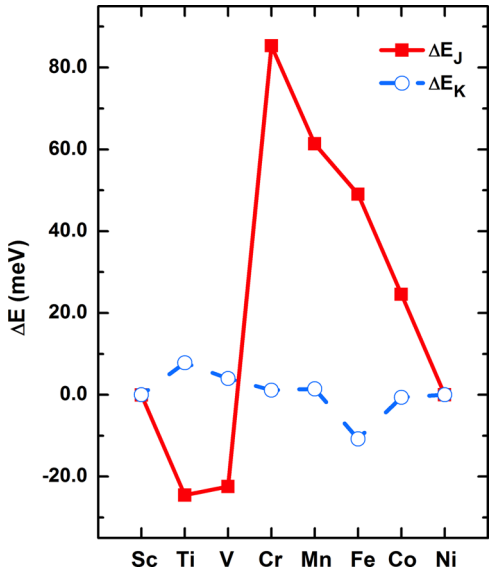


**Figure 4.** $\Delta E$ in $[T_{1/4}WSe_2]_8$. The solid (red) lines represent $\Delta E$ without SOC ($\Delta E_J$), and the dashed (blue) lines represent the anisotropic contribution to $\Delta E$ due to SOC ($\Delta E_K$). Here, $\Delta E_i = E_i^{AFM} - E_i^{FM}$, where ($i$ = $J$ and $K$).

0.81 $\mu_B$, for Ti, V, Cr, Mn, Fe, and Co, are similar to the FM moments discussed above. This indicates that the system is somewhat anisotropic but otherwise nearly Heisenberg magnet, with moments nearly independent of the angle between neighboring spins.

The calculated $\Delta E$ in the absence of SOC for Cr, Mn, and Fe intercalates in $WSe_2$ are 85.3, 61.3, and 49.0 meV, whereas the total $\Delta E$ for Cr, Mn, and Fe after including SOC are 86.4, 62.7, and 38.2 meV, respectively. From these values, we infer that the anisotropic spin−orbit coupling effect is relativistically small and normally a minor correction to the leading isotropic Heisenberg exchange through $WSe_2$ layers. However, it becomes more important if the isotropic Heisenberg exchange is small by coincidence, for example in the vicinity of an FM−AFM transition. Figure 4 shows this case for the early transition metals (Sc, Ti, and V) in $T_{1/4}WSe_2$. Furthermore, to check the robustness of the magnetic order with respect to correlations, we performed DFT + $U$ calculations for two different values of $U$. We find that $U$ does not affect the magnetic order in these systems.

It is interesting to evaluate the magnetic ordering temperature, that is, the Curie temperature ($T_C$) in the ferromagnetic case. We use mean-field expression

$$T_C = \frac{2}{3k_B}(\Delta E) \quad (2)$$

where the energy difference refers to the switching of one T spin per supercell, as shown in Figure 4. We estimate $T_C$ values of 660, 475, 379, and 189 K for Cr, Mn, Fe, and Co, respectively. The values for Cr, Mn, and Co may be useful for devices that operate at room temperature.[37,38]

Apart from yielding a correction to the energy of FM and AFM states, the SOC is responsible for the orbital moment contribution to the total magnetic moment and magnetocrystalline anisotropy. The anisotropy energy, $E_{MCA}$, is obtained as

$$E_{MCA} = E_x - E_z \quad (3)$$

where $E_x$ and $E_z$ are the respective self-consistent total DFT energies when the magnetization is in the film plane ($E_x$) and parallel to the $c$- or $z$-direction perpendicular to the film ($E_z$).[39] To calculate the AFM anisotropy energy, the spins of the two T atoms in the supercell are aligned antiparallel to each other.

Figure 5 shows the orbital moment and the anisotropy energy in their minimum-energy spin structures, using $U$ = 0.

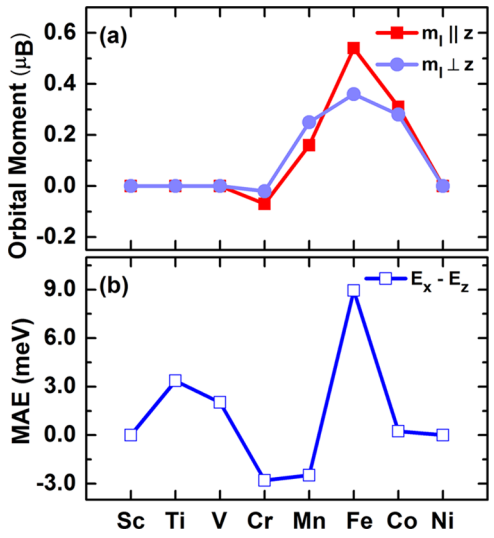


**Figure 5.** Effect of spin−orbit interactions in intercalated $WSe_2$: (a) transition metal orbital moments along two magnetization directions and (b) magnetocrystalline anisotropy energy (MAE or $E_{MCA}$) ~ $K_1$, measured in meV per supercell.

The orbital moment on the W atoms is very small and therefore not shown. Note that W has a relatively strong spin−orbit coupling, but the net orbital moment of the W atoms is proportional to the induced W spin moment and therefore strongly reduced. For Ti, V, Cr, and Mn intercalates, the orbital moments are small, in the range of 0.1−0.25 $\mu_B$ per supercell. Figure 5a shows the plot of total orbital moment of the system along the $x$- and $z$-direction. Ti- and V-intercalated $WSe_2$ exhibit AFM order structure, as discussed above in Figure 4, which results in zero total orbital moment. In case of Cr and Mn, the orbital moment is largest in the $WSe_2$ plane and the magnetocrystalline anisotropy is of the easy-plane type ($K_1$ < 0), whereas for Ti, V, Mn, Fe, and Co intercalates, the total orbital moment is largest in the plane perpendicular to the $WSe_2$ plane, which suggests an out-of-plane anisotropy. Among the iron-series intercalates, a significantly large perpendicular orbital moment of 0.55 $\mu_B$ has been found for the Fe intercalate, and the resulting orbital moment anisotropy of 0.2 $\mu_B$ (Figure 5a) indicates strong perpendicular anisotropy. Indeed, Figure 5b shows that $Fe_{1/4}WSe_2$ exhibits a large anisotropy constant of 9.0 meV per supercell.

## 3. CONCLUSIONS

In summary, we have investigated the effect of 3d metal atom intercalation on the electronic and magnetic properties of $WSe_2$. The spin structure depends on the intercalated transition-metal atom and changes from antiferromagnetism at the beginning of the series to strong ferromagnetism for the later transition metals. The high moments are also accompanied by high Curie temperatures. Iron intercalation yields a strong perpendicular magnetocrystalline anisotropy of 9.0 meV



DOI: 10.1021/acsomega.7b01164
ACS Omega 2017, 2, 7985−7990

per supercell. Our calculations indicate that Ti and V create delocalized antiferromagnetism, whereas Cr, Mn, Fe, and Co exhibit localized ferromagnetism in $WSe_2$. The magnetic moment, the high Curie temperatures, and the high magnetic anisotropy suggest that these late iron-series transition-metal atoms intercalated in $WSe_2$ may have potential applications in spin electronics and quantum-information devices.

## 4. COMPUTATIONAL DETAILS

The first-principles calculations were carried out within the framework of density functional theory (DFT), as implemented in the Vienna ab initio simulation package.[40,41] Within the generalized gradient approximation, we use projector augmented wave pseudopotentials with exchange and correlation effects described by the Perdew−Burke and Ernzerhof (PBE) functional.[42] To accurately describe the wave functions, a plane-wave cutoff of 520 eV is used. To account for the dispersion interactions of van der Waals in layered compounds, we optimized the lattice parameters of pure $WSe_2$ using the semiempirical London dispersion correction of Grimme et al.[43] Considering this correction, the optimized lattice parameters of pure $WSe_2$ are found to be $a = b = 3.29$ Å and $c = 13.023$ Å, which agree fairly well with earlier findings.[44,45] For $WSe_2$, we find a band gap of 1.02 eV, which is comparable to the existing literature.[46]

The lattice parameters and atomic positions are fully optimized using a Γ-centered $k$-mesh of size $7 \times 7 \times 5$ until the forces on each of the atoms are below 2.0 meV/Å. For the self-consistent field calculations, a mesh of size $13 \times 13 \times 7$ is used with an energy convergence threshold of $10^{-6}$ eV. A DFT + $U$ scheme is employed to estimate the electron correlations of the iron-series 3d electrons, using $U = 3$ and 7 eV and $J = 1$ eV in addition to the uncorrelated case ($U = 0$).

To calculate the magnetocrystalline anisotropy, the spin−orbit coupling (SOC) is included in a noncollinear mode,[47,48] using an energy convergence threshold of 1 μeV and a Γ-centered $k$-mesh of $15 \times 15 \times 9$ to sample the Brillouin zone of the system.[49]

## AUTHOR INFORMATION


### Corresponding Author

*E-mail: pankajsahota@gmail.com.

### ORCID

Pankaj Kumar: 0000-0002-9024-8899


### Notes

The authors declare no competing financial interest.

## ACKNOWLEDGMENTS

We gratefully acknowledge financial support from the NSF CAREER award (DMR-1255584) and Research Corporation's Cottrell College Science award (Grant No. 20234). The contribution by R.S. has been partially supported by DOE BES (04ER46152). The computational support for the project is provided by the HPC center of Idaho National Laboratory and Extreme Science and Engineering Discovery Environment (XSEDE), which is supported by National Science Foundation grant number ACI-1548562.

## REFERENCES

(1) Tedstone, A. A.; Lewis, D. J.; O'Brien, P. Synthesis, Properties, and Applications of Transition Metal-Doped Layered Transition Metal Dichalcogenides. *Chem. Mater.* **2016**, 1965−1974.

(2) Wang, Q. H.; Kalantar-Zadeh, K.; Kis, A.; Coleman, J. N.; Strano, M. S. Electronics and Optoelectronics of Two-Dimensional Transition Metal Dichalcogenides. *Nat. Nanotechnol.* **2012**, *7*, 699−712.

(3) Duan, X.; Wang, C.; Pan, A.; Yu, R.; Duan, X. Two-Dimensional Transition Metal Dichalcogenides as Atomically Thin Semiconductors: Opportunities and Challenges. *Chem. Soc. Rev.* **2015**, *44*, 8859−8876.

(4) Xu, X.; Yao, W.; Xiao, D.; Heinz, T. F. Spin and Pseudospins in Layered Transition Metal Dichalcogenides. *Nat. Phys.* **2014**, *10*, 343−350.

(5) Wan, J.; Lacey, S. D.; Dai, J.; Bao, W.; Fuhrer, M. S.; Hu, L. Tuning Two-Dimensional Nanomaterials by Intercalation: Materials, Properties and Applications. *Chem. Soc. Rev.* **2016**, *45*, 6742−6765.

(6) Zhou, Y.; Yang, P.; Zu, H.; Gao, F.; Zu, X. Electronic Structures and Magnetic Properties of $MoS_2$ Nanostructures: Atomic Defects, Nanoholes, Nanodots and Antidots. *Phys. Chem. Chem. Phys.* **2013**, *15*, 10385−10394.

(7) Shu, H.; Luo, P. F.; Liang, P.; Cao, D.; Chen, X. S. Layer-Dependent Dopant Stability and Magnetic Exchange Coupling of Iron-Doped $MoS_2$ Nanosheets. *ACS Appl. Mater. Interfaces* **2015**, *7*, 7534−7541.

(8) Manchanda, P.; Skomski, R. 2D Transition-Metal Diselenides: Phase Segregation, Electronic Structure, and Magnetism. *J. Phys.: Condens. Matter* **2016**, *28*, No. 064002.

(9) Gil, C. J.; Pham, A.; Yu, A.; Li, S. An Ab Initio Study of Transition Metals Doped with $WSe_2$ for Long-Range Room Temperature Ferromagnetism in Two-Dimensional Transition Metal Dichalcogenide. *J. Phys.: Condens. Matter* **2014**, *26*, No. 306004.

(10) Andriotis, A. N.; Menon, M. Tunable Magnetic Properties of Transition Metal Doped $MoS_2$. *Phys. Rev. B* **2014**, *90*, No. 125304.

(11) Cha, J. J.; Koski, K. J.; Huang, K. C. Y.; Wang, K. X.; Luo, W.; Kong, D.; Yu, Z.; Fan, S.; Brongersma, M. L.; Cui, Y. Two-Dimensional Chalcogenide Nanoplates as Tunable Metamaterials via Chemical Intercalation. *Nano Lett.* **2013**, *13*, 5913−5918.

(12) Jung, Y.; Zhou, Y.; Cha, J. J. Intercalation in Two-Dimensional Transition Metal Chalcogenides. *Inorg. Chem. Front.* **2016**, *3*, 452−463.

(13) Ko, K. T.; Kim, K.; Kim, S. B.; Kim, H. D.; Kim, J. Y.; Min, B. I.; Park, J. H.; Chang, F. H.; Lin, H. J.; Tanaka, A.; et al. RKKY Ferromagnetism with Ising-like Spin States in Intercalated $Fe_{1/4}TaS_2$. *Phys. Rev. Lett.* **2011**, *107*, No. 247201.

(14) Manchanda, P.; Sharma, V.; Yu, H.; Sellmyer, D. J.; Skomski, R. Magnetism of Ta Dichalcogenide Monolayers Tuned by Strain and Hydrogenation. *Appl. Phys. Lett.* **2015**, *107*, No. 032402.

(15) Yang, S.; Wang, C.; Sahin, H.; Chen, H.; Li, Y.; Li, S. S.; Suslu, A.; Peeters, F. M.; Liu, Q.; Li, J.; et al. Tuning the Optical, Magnetic, and Electrical Properties of $ReSe_2$ by Nanoscale Strain Engineering. *Nano Lett.* **2015**, *15*, 1660−1666.

(16) Zhou, Y.; Wang, Z.; Yang, P.; Zu, X.; Yang, L.; Sun, X.; Gao, F. Tensile Strain Switched Ferromagnetism in Layered $NbS_2$ and $NbSe_2$. *ACS Nano* **2012**, *6*, 9727−9736.

(17) Guo, H.; Lu, N.; Wang, L.; Wu, X.; Zeng, X. C. Tuning Electronic and Magnetic Properties of Early Transition-Metal Dichalcogenides via Tensile Strain. *J. Phys. Chem. C* **2014**, *118*, 7242−7249.

(18) Friend, R. H.; Beal, A. R.; Yoffe, A. D. Electrical and Magnetic Properties of Some First Row Transition Metal Intercalates of Niobium Disulphide. *Philos. Mag.* **1977**, *35*, 1269−1287.

(19) Mankovsky, S.; Chadova, K.; Ködderitzsch, D.; Minár, J.; Ebert, H.; Bensch, W. Electronic, Magnetic, and Transport Properties of Fe-Intercalated 2H-$TaS_2$ Studied by Means of the KKR-CPA Method. *Phys. Rev. B* **2015**, *92*, No. 144413.

(20) Choi, Y. J.; Kim, S. B.; Asada, T.; Park, S.; Wu, W.; Horibe, Y.; Cheong, S.-W. Giant Magnetic Coercivity and Ionic Superlattice Nano-Domains in $Fe_{0.25}TaS_2$. *Europhys. Lett.* **2009**, *86*, 37012.

(21) Hardy, W. J.; Chen, C. W.; Marcinkova, A.; Ji, H.; Sinova, J.; Natelson, D.; Morosan, E. Very Large Magnetoresistance in $Fe_{0.28}TaS_2$ Single Crystals. *Phys. Rev. B: Condens. Matter Mater. Phys.* **2015**, *91*, 54426.



DOI: 10.1021/acsomega.7b01164
*ACS Omega* 2017, 2, 7985−7990

(22) Shand, P. M.; Cooling, C.; Mellinger, C.; Danker, J. J.; Kidd, T. E.; Boyle, K. R.; Strauss, L. H. Magnetic States in Nanostructured Manganese-Intercalated $TaS_2$. *J. Magn. Magn. Mater.* **2015**, *382*, 49−57.
(23) Bruno, P. Tight-Binding Approach to the Orbital Magnetic Moment and Magnetocrystalline Anisotropy of Transition-Metal Monolayers. *Phys. Rev. B* **1989**, *39*, 865−868.
(24) Skomski, R.; Kashyap, A.; Enders, A. Is the Magnetic Anisotropy Proportional to the Orbital Moment? *J. Appl. Phys.* **2011**, *109*, No. 07E143.
(25) Le, D.; Barinov, A.; Preciado, E.; Isarraraz, M.; Tanabe, I.; Komesu, T.; Troha, C.; Bartels, L.; Rahman, T. S.; Dowben, P. A. Spin−orbit Coupling in the Band Structure of Monolayer WSe2. *J. Phys.: Condens. Matter* **2015**, *27*, No. 182201.
(26) Yuan, H.; Bahramy, M. S.; Morimoto, K.; Wu, S.; Nomura, K.; Yang, B.-J.; Shimotani, H.; Suzuki, R.; Toh, M.; Kloc, C.; et al. Zeeman-Type Spin Splitting Controlled by an Electric Field. *Nat. Phys.* **2013**, *9*, 563−569.
(27) Nourbakhsh, A.; Zubair, A.; Dresselhaus, M. S.; Palacios, T. Transport Properties of a $MoS_2/WSe_2$ Heterojunction Transistor and Its Potential for Application. *Nano Lett.* **2016**, *16*, 1359−1366.
(28) Flöry, N.; Jain, A.; Bharadwaj, P.; Parzefall, M.; Taniguchi, T.; Watanabe, K.; Novotny, L. A $WSe_2/MoSe_2$ Heterostructure Photovoltaic Device. *Appl. Phys. Lett.* **2015**, *107*, No. 123106.
(29) Groenendijk, D. J.; Buscema, M.; Steele, G. A.; Michaelis De Vasconcellos, S.; Bratschitsch, R.; Van Der Zant, H. S. J.; Castellanos-Gomez, A. Photovoltaic and Photothermoelectric Effect in a Double-Gated $WSe_2$ Device. *Nano Lett.* **2014**, *14*, 5846−5852.
(30) Peng, Q.; Wang, Z.; Sa, B.; Wu, B.; Sun, Z.; Novoselov, K. S.; Liu, H.; Sa, B.; Li, Y. L.; Qi, J.; et al. Electronic Structures and Enhanced Optical Properties of Blue Phosphorene/transition Metal Dichalcogenides van Der Waals Heterostructures. *Sci. Rep.* **2016**, *6*, No. 31994.
(31) Tonndorf, P.; Schmidt, R.; Böttger, P.; Zhang, X.; Börner, J.; Liebig, A.; Albrecht, M.; Kloc, C.; Gordan, O.; Zahn, D. R. T.; et al. Photoluminescence Emission and Raman Response of Monolayer $MoS_2$, $MoSe_2$, and $WSe_2$. *Opt. Express* **2013**, *21*, 4908−4916.
(32) Andersen, A.; Kathmann, S. M.; Lilga, M. A.; Albrecht, K. O.; Hallen, R. T.; Mei, D. First-Principles Characterization of Potassium Intercalation in Hexagonal 2H-$MoS_2$. *J. Phys. Chem. C* **2012**, *116*, 1826−1832.
(33) Reshak, A. H.; Auluck, S.; Majchrowski, A.; Kityk, I. <tep-common:author-query>AQ3: Please provide a DOI number for ref 33 or indicate if one doesn’t exist.</tep-common:author-query>Comparison of the Density of States Obtained from the X-Ray Photoelectron Spectra with the Electronic Structure Calculations for BiB<sub>3</sub>O<sub>6</sub>. *Jpn. J. Appl. Phys.* **2009**, *48*, 11601.
(34) Tang, W.; Sanville, E.; Henkelman, G. A Grid-Based Bader Analysis Algorithm without Lattice Bias. *J. Phys.: Condens. Matter* **2009**, *21*, No. 084204.
(35) Sims, H.; Oset, S. J.; Butler, W. H.; MacLaren, J. M.; Marsman, M. Determining the Anisotropic Exchange Coupling of $CrO_2$ via First-Principles Density Functional Theory Calculations. *Phys. Rev. B* **2010**, *81*, 1−9.
(36) Kan, M.; Adhikari, S.; Sun, Q. Ferromagnetism in $MnX_2$ (X = S, Se) Monolayers. *Phys. Chem. Chem. Phys.* **2014**, *16*, 4990−4994.
(37) Pajda, M.; Kudrnovský, J.; Turek, I.; Drchal, V.; Bruno, P. *Ab-Initio* Calculations of Exchange Interactions, Spin-Wave Stiffness Constants, and Curie Temperatures of Fe, Co, and Ni. *Phys. Rev. B* **2001**, *64*, No. 174402.
(38) Kittel, C. *Introduction to Solid State Physics*; John Wiley & Sons: New York, 1996.
(39) Błoński, P.; Hafner, J. Density-Functional Theory of the Magnetic Anisotropy of Nanostructures: An Assessment of Different Approximations. *J. Phys.: Condens. Matter* **2009**, *21*, No. 426001.
(40) Kresse, G.; Furthmüller, J. Efficient Iterative Schemes for *Ab-Initio* Total-Energy Calculations Using a Plane-Wave Basis Set. *Phys. Rev. B* **1996**, *54*, 11169−11186.
(41) Kresse, G.; Joubert, D. From Ultrasoft Pseudopotentials to the Projector Augmented-Wave Method. *Phys. Rev. B* **1999**, *59*, 1758−1775.
(42) Perdew, J. P.; Burke, K.; Ernzerhof, M. Generalized Gradient Approximation Made Simple. *Phys. Rev. Lett.* **1996**, *77*, 3865−3868.
(43) Grimme, S.; Antony, J.; Ehrlich, S.; Krieg, H. A Consistent and Accurate Ab Initio Parametrization of Density Functional Dispersion Correction (DFT-D) for the 94 Elements H-Pu. *J. Chem. Phys.* **2010**, *132*, No. 154104.
(44) Traving, M.; Boehme, M.; Kipp, L.; Skibowski, M.; Starrost, F.; Krasovskii, E. E.; Perlov, A.; Schattke, W. Electronic Structure of $WSe_2$: A Combined Photoemission and Inverse Photoemission Study. *Phys. Rev. B* **1997**, *55*, 10392−10399.
(45) Kormányos, A.; Burkard, G.; Gmitra, M.; Fabian, J.; Zólyomi, V.; Drummond, N. D.; Fal'ko, V. K.p Theory for Two-Dimensional Transition Metal Dichalcogenide Semiconductors. *2D Mater.* **2015**, *2*, No. 022001.
(46) Kumar, A.; Ahluwalia, P. K. Electronic Structure of Transition Metal Dichalcogenides Monolayers 1H-$MX_2$ (M = Mo, W; X = S, Se, Te) from *Ab-Initio* Theory: New Direct Band Gap Semiconductors. *Eur. Phys. J. B* **2012**, *85*, 186.
(47) Hobbs, D.; Kresse, G.; Hafner, J. Fully Unconstrained Noncollinear Magnetism within the Projector Augmented-Wave Method. *Phys. Rev. B: Condens. Matter Mater. Phys.* **2000**, *62*, 11556−11570.
(48) Marsman, M.; Hafner, J. Broken Symmetries in the Crystalline and Magnetic Structures of $\gamma$ -Iron. *Phys. Rev. B* **2002**, *66*, No. 224409.
(49) Pack, J. D.; Monkhorst, H. J. "Special Points for Brillouin-Zone Integrations"-a Reply. *Phys. Rev. B* **1977**, *16*, 1748−1749.


DOI: 10.1021/acsomega.7b01164
*ACS Omega* 2017, 2, 7985−7990